Mathematical and Computational Applications

MDPI

Article

Geometric Modeling and 3D Printing Using Recursively Generated Point Cloud

Tashi [1], **AMM Sharif Ullah** [2,*] and **Akihiko Kubo** [2]

[1] Graduate School of Engineering, Kitami Institute of Technology, 165 Koen-cho, Kitami 090-8507, Japan; tashi.cst@rub.edu.bt

[2] Faculty of Engineering, Kitami Institute of Technology, 165 Koen-cho, Kitami 090-8507, Japan; kuboak@mail.kitami-it.ac.jp

* Correspondence: ullah@mail.kitami-it.ac.jp; Tel./Fax: +81-157-26-9207

Received: 15 June 2019; Accepted: 16 September 2019; Published: 17 September 2019

Abstract: Previous studies have reported that a recursive process called the point cloud creation algorithm (PCA) that generates a point cloud is useful for reverse engineering a planner shape. This study elucidates the characteristics of the parameters used in the recursive process as well as its ability in geometric modeling and 3D printing of 3D shapes. In the recursive process, three constants (center point, initial distance, and initial angle) and two variables (instantaneous distance and instantaneous rotational angle) are employed. The shape-modeling characteristics of the constants and variables are elucidated using some commonly used shapes (straight-line, circle, ellipses, spiral, astroid, S-shape, and leaf-shape). In addition, the shape-modeling capability of the recursive process as a whole is quantified using two parameters called the radius of curvature and aesthetic value. Moreover, an illustrative example that shows the efficacy of the recursive process in virtual and physical prototyping of a relatively complex 3D object is presented. The results show that reverse engineering performed by the recursive-process-created point cloud is free from computational complexity compared to reverse engineering performed by the 3D-scanner-created point cloud. As such, the outcomes of this study enrich the field of reverse engineering.

Keywords: geometric modeling; additive manufacturing; reverse engineering; point cloud; design for additive manufacturing

1. Introduction

Additive manufacturing (AM) (in common terms, 3D printing) has emerged as a useful process for producing complex shapes directly from the solid 3D CAD models of the shapes [1–7]. Numerous industrial sectors have been benefitting from AM, including the automotive industry [8], the aerospace industry [1], the biomedical engineering field (e.g., dental braces, artificial tissues, hearing aids, dummy cadavers, and prosthetics) [9–15], the education field [16–18], the fashion industry (e.g., cloth, shoes, and jewelry) [19–23], the food industry (e.g., pizza, chocolate, crackers, and pasta) [24–28], and the construction industry (e.g., 3D printed houses) [29–32]. AM has also been applied to preserving and restoring cultural heritage [33]. Thus, the advent of AM has created a new field called Design for Additive Manufacturing (DfAM). One of the objectives of DfAM is to manage the complexity in the geometry and topology of a given object for the ease of AM [34].

The typical steps underlying an AM process are Steps 4 to 7, as shown in Figure 1. In some cases, particularly when a given object is reverse engineered [35–37], Steps 1 to 3 in Figure 1 must be added to make the process meaningful. Therefore, some of the challenges of DfAM are rooted in Steps 2 and 3, as described below.

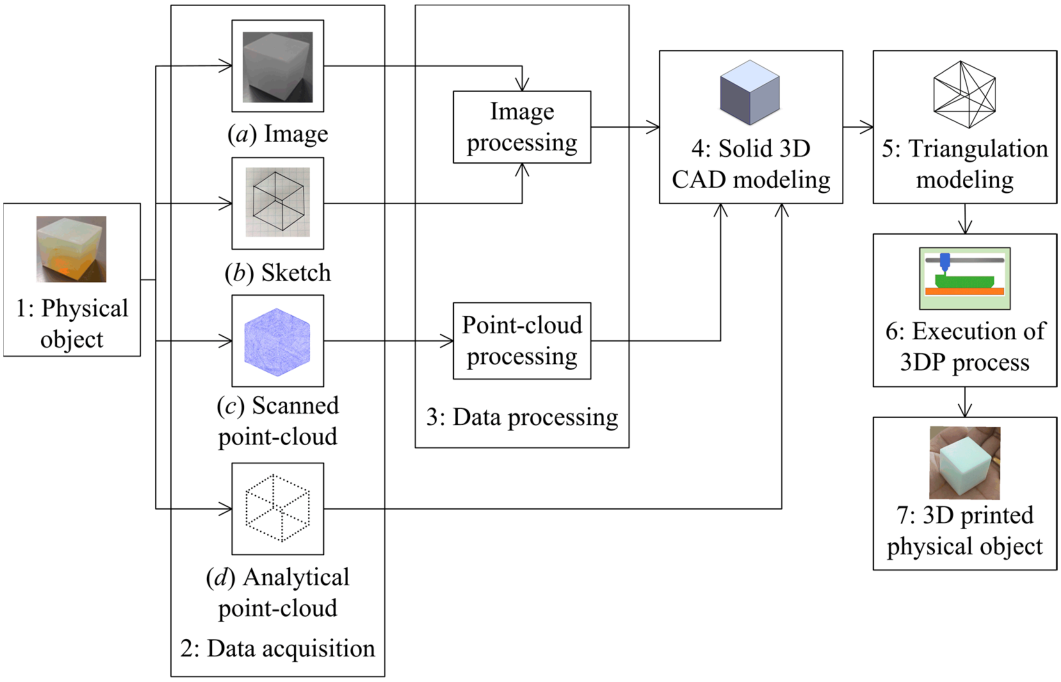

Figure 1. Additive manufacturing from the viewpoint of reverse engineering.

When a given object is reverse engineered, a data acquisition process is required, as shown by Step 2. In most cases, data acquisition is based on image processing, sketch processing, scanned point cloud processing, or analytical point cloud processing. In the case of image processing, the image data of a given object are extracted. Afterward, the data are processed by an appropriate computational method (Step 3) for making the information meaningful to a CAD package for solid modeling. In the case of sketch processing, a given object is sketched and then the sketch data are processed by an appropriate computational method for making the information meaningful to a CAD package for solid modeling. In the case of scanned point-cloud processing, a given object is scanned by a 3D scanner and then represented by a relatively large set of points known as a point cloud. Afterward, the point cloud is processed by an appropriate computational method for making the information meaningful to a CAD package for solid modeling. Thus, the abovementioned data acquisition processes require either image processing or point cloud processing. The computational complexity and the respective solutions have been studied by numerous authors, as reported in [38]. For the sake of better understanding, the following articles can be noted that show the computational details regarding raster to vector graphics conversion [39–41], sketch processing [42–44], data registration [9,45–47], noise removal [48,49], data reduction [50,51], curve-based surface reconstruction [42,52–58], polygon-based surface reconstruction [59–63], and direct slicing [64–68].

Compared to the image processing, sketch processing, and scanned point-cloud processing, analytical-point-cloud-processing-based reverse engineering is still in infancy. However, one of the advantages of analytical-point-cloud-based reverse engineering is that it can restrict the size of the point cloud to a small one. This way, some of the computational complexity as mentioned above can be avoided, as shown by the authors in [69]. On the other hand, there is an inherent problem, that is, what is the best approach to create an analytical point cloud? In this regard, there are multiple approaches. An analytical point cloud can be created using a deterministic approach [38,70], a semi-random approach or affine mapping-based approach [34,71], and a fully random approach [72]. In each case, the 3D solid model construction process can be systematized using the information underlying the analytically created point cloud. This is perhaps not the case when the other approaches are used to create the point cloud.

In this article, the focus is on the deterministic point cloud that is created by a recursive process as shown in [38,69,70]. This process uses two variables and three constants, which are user-defined. The role and the characteristics of these variables and constants must be known beforehand to facilitate the modeling process. Whether or not a given shape has been modeled as per the requirement has not been elucidated yet. The deterministic point cloud creation process has been applied to modeling the planner shapes only. Therefore, the following questions are yet to be answered.

- What are the characteristics and roles of the variables and constants used in the recursive process that deterministically creates a point cloud?
- How do we quantify the shape information modeled by a set of a point cloud?
- Does the recursive process that deterministically creates a point cloud correctly model a given shape?
- Does the deterministically created point cloud help create 3D solid models of some given objects?

This article addresses answers to the aforementioned questions. The rest of the article is organized as follows. Section 2 describes the characteristics of the point-cloud-creating algorithm. Section 3 describes the quantification of point cloud by the radius of curvature and aesthetic value. Section 4 describes the 3D solid modeling and physical prototyping of a given shape guided by some points. Section 5 describes the discussion on a point-cloud-based surface texturing and processing of point cloud obtained from a 3D scanner. Section 5 provides the concluding remarks of this study.

2. Characteristics of the Point-Cloud-Creating Algorithm

Recall the following question. What are the characteristics and roles of the variables and constants used in the recursive process that deterministically creates a point cloud? The recursive process, called the point cloud creation algorithm (PCA), that creates a point cloud on a plane is shown in Appendix A. As shown in Appendix A, PCA needs three constants as inputs—namely, the center point, P_c; initial distance, d; and initial angle, φ—that remain the same for all iterations. In addition, PCA needs two variables as inputs—namely, instantaneous rotational angle, θ_i and instantaneous distance, r_i, $i = 0, 1, ..., n$—that may change in every iteration. The PCA creates the output, denoted as $PC = \{P_{ei} \mid i = 0, 1, ..., n\}$, which is a small-size point cloud. As such, the output of PCA, PC depends on d, φ, θ_i, and r_i. This input–output relationship is characterized by using some well-known shapes, namely, straight-line, circle, ellipse, spiral, astroid, S-shape, and leaf-shape. The description is as follows.

First, consider the point clouds that evolve due to the linear settings of the instantaneous rotational angle and distance. These settings create some point clouds presenting straight lines, circles, and spirals, as shown in Figures 2–5. For example, consider a point cloud that models a straight line. In this case, θ_i must be kept constant and r_i must linearly increase or decrease. When $\theta_i = 0°$ and r_i linearly increases for all iterations, the PCA creates a point cloud, PC, presenting a horizontal line, as shown in Figure 2. When $\theta_i = 90°$ and r_i linearly increases for all iterations, the PCA creates, PC, presenting a vertical line, as shown in Figure 3. The slope of the straight line can be modeled using θ_i. When an opposite strategy is adopted, that is, θ_i is increased or decreased linearly and r_i is kept constant, the point cloud, PC, presents a shape called a circle, as shown in Figure 4. In this case, the radius of the circle can be modeled using r_i. On the other hand, when both θ_i and r_i are increased or decreased simultaneously, then the point cloud, PC, presents a shape called a spiral, as shown in Figure 5.

In the next step, consider the relatively complex settings of the instantaneous distance while keeping the instantaneous rational angle increase linear. For example, when θ_i is increased linearly and r_i follows a tent function, then the point cloud, PC, presents a shape called leaf-shape, as shown in Figure 6. When θ_i increases linearly and r_i follows a sine or cosine function with two cycles, then the point cloud, PC, presents a shape called ellipse, as shown in Figure 7. Similarly, when θ_i increases linearly and r_i follows a u-shape function with four cycles, then the point cloud, PC, presents a shape called astroid, as shown in Figure 8. When θ_i increases linearly and r_i follows a bathtub function with two cycles, then the point cloud, PC, presents a shape called S-shape, as shown in

Figure 9. As shown in Figures 2–9, keeping θ_i very simple (constant or straight-line) and varying r_i using some simple functions (straight-line, tent function, sine/cosine, u-shape function, and bathtub functions) can model a variety of shapes. The findings are summarized in Table 1. These characteristics of the algorithm can be used while modeling an arbitrary planner shape or a segment of it.

As shown in Table 1, besides the instantaneous rotational angle and distance described above, the other input parameters of the PCA, the center point, P_c and the initial angle, φ also play an important role. For instance, the leaf-shape shown in Figure 9 can be rotated by resetting the values of φ. For example, when the initial angle is set in the following manner φ = 0°, 45°, and 90°, the leaf-shape shown in Figure 6 rotates by 0°, 45°, and 90°, respectively, as shown in Figure 10. Similarly, P_c can perform the function of translation in both x-axis and y-axis directions. The initial distance, d, on the other hand, does not play many roles, i.e., it does not affect the shape to be modeled; it is only necessary for placing the starting point.

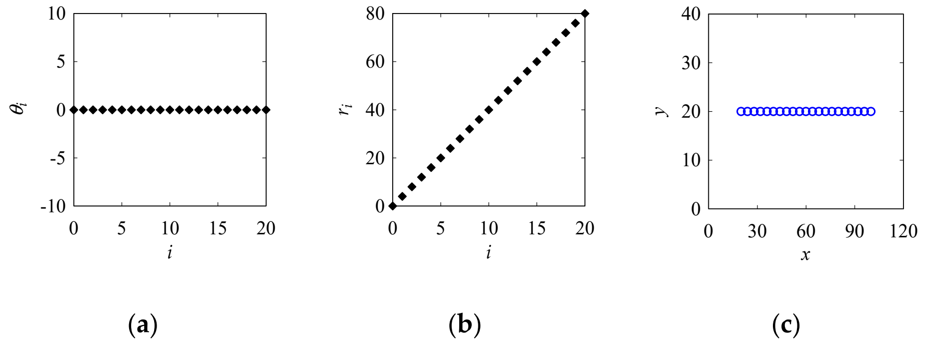

(**a**) (**b**) (**c**)

Figure 2. Settings for a horizontal straight line using the point cloud creation algorithm (PCA). (**a**) Input1: θ_i; (**b**) Input2: r_i; (**c**) Output: Point cloud.

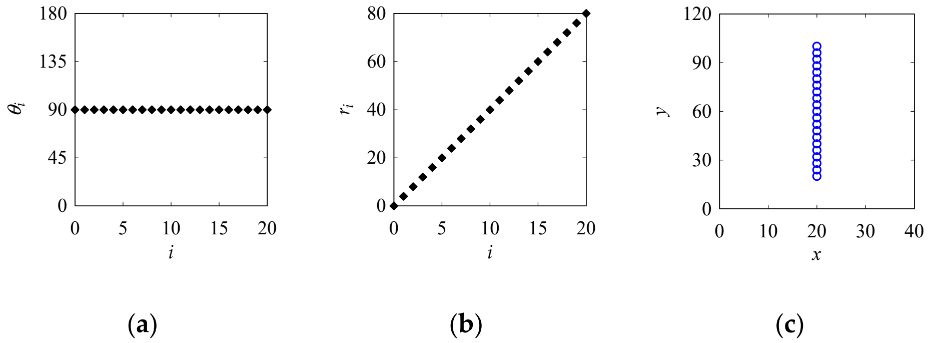

(**a**) (**b**) (**c**)

Figure 3. Settings for a vertical straight line using the PCA. (**a**) Input1: θ_i; (**b**) Input2: r_i; (**c**) Output: Point cloud.

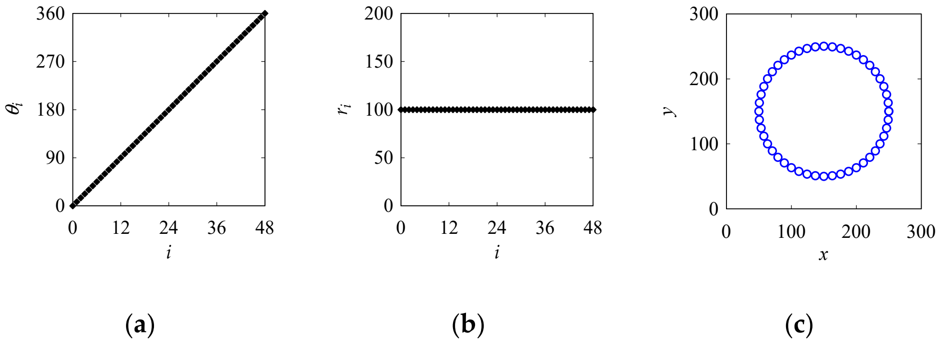

(**a**) (**b**) (**c**)

Figure 4. Settings for a circle using the PCA. (**a**) Input1: θ_i; (**b**) Input2: r_i; (**c**) Output: Point cloud.

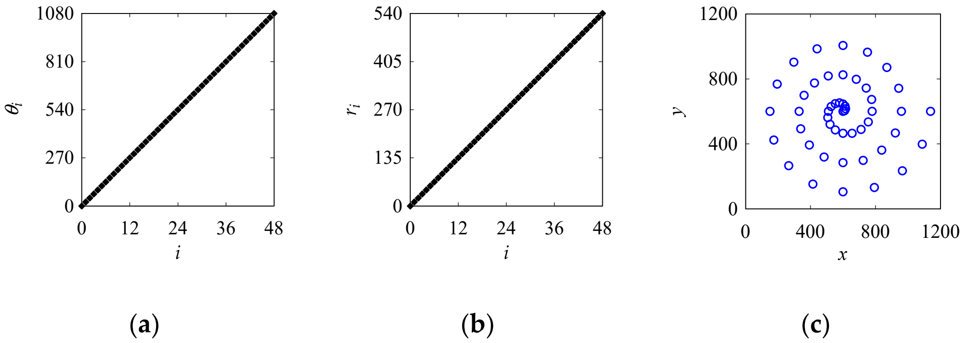

Figure 5. Settings for a spiral using the PCA. (**a**) Input1: θ_i; (**b**) Input2: r_i; (**c**) Output: Point cloud.

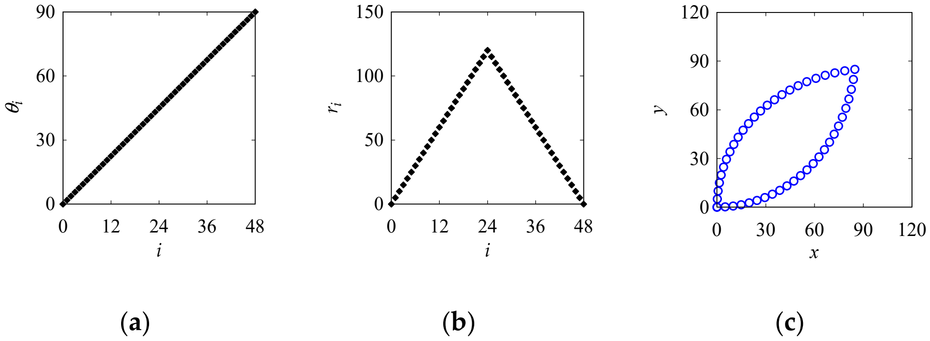

Figure 6. Settings for a leaf-shape using the PCA. (**a**) Input1: θ_i; (**b**) Input2: r_i; (**c**) Output: Point cloud.

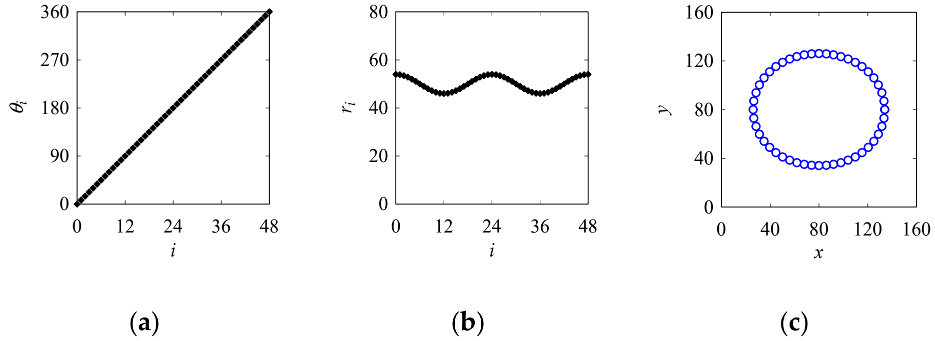

Figure 7. Settings for an ellipse using the PCA. (**a**) Input1: θ_i; (**b**) Input2: r_i; (**c**) Output: Point cloud.

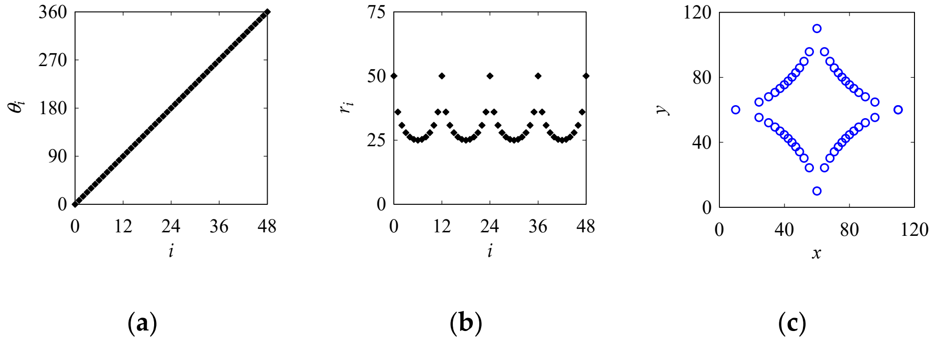

Figure 8. Settings for an astroid using the PCA. (**a**) Input1: θ_i; (**b**) Input2: r_i; (**c**) Output: Point cloud.

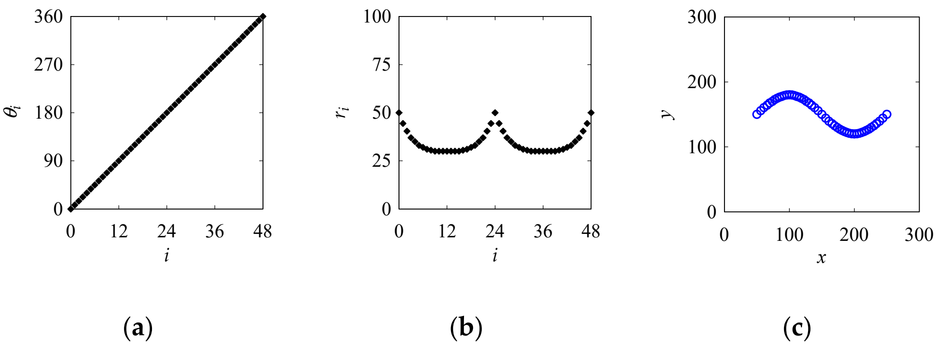

Figure 9. Settings for an S-shape using the PCA. (**a**) Input1: θ_i; (**b**) Input2: r_i; (**c**) Output: Point cloud of half of an S-shape.

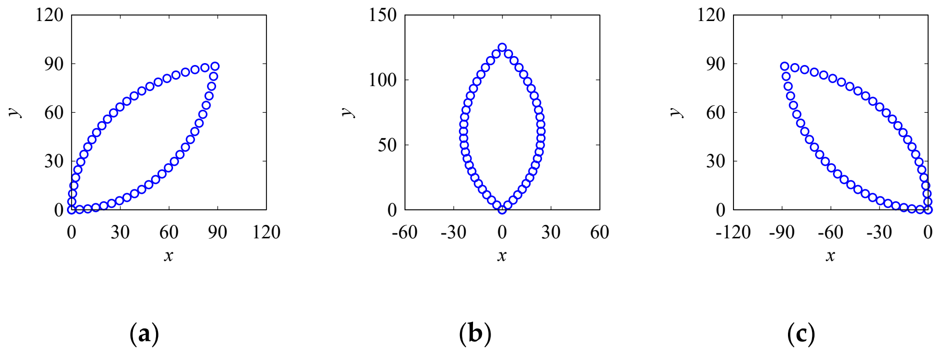

Figure 10. Role of an Initial Angle. (**a**) When $\varphi = 0°$; (**b**) when $\varphi = 45°$; (**c**) when $\varphi = 90°$.

Table 1. Summary of the characteristics of the point-cloud-creation algorithm.

Instantaneous Rotational Angle, θ_i	**Instantaneous Distance, r_i**	**Point Cloud, *PC***
Constant	Increase or decrease linearly	Straight-line
Increase or decrease linearly	Constant	Circle
	Increases linearly	Spiral
	Increase and decrease linearly like a tent function	Leaf-shape
	Decrease and increase gradually like a sine/cosine for two cycles	Ellipse
	Decrease and increase gradually like a U-shape function for four cycles	Astroid
	Decrease and increase gradually like a bathtub function for two cycles	S-shape
Center point, P_c		Translate a shape
Initial angle, φ		Rotate shape
Initial distance, d		No effect on a shape

3. Quantification of Point Clouds

Recall the following questions. How do we quantify the shape information modeled by a set of a point cloud? Does the recursive process that deterministically creates a point cloud correctly model a given shape?

In order to answer the abovementioned questions, two well-known parameters called a radius of curvature and aesthetic value, defined in Appendix B, are considered.

Let A be a planner shape. Let U be a method that creates a point cloud $V = \{V_i \mid i = 0, 1, \ldots\}$ to model A. In addition, $PC = \{P_{ei} \mid i = 0, 1, ...\}$ is created by PCA to model A. As such, both point clouds, $V = \{V_i \mid i = 0, 1, \ldots\}$ and $PC = \{P_{ei} \mid i = 0, 1, ...\}$ must look alike. At the same time, their quantitative characteristics must be the same. Based on this consideration, this section quantifies two point clouds of the same shape using the radius of curvature and aesthetic value, respectively.

3.1. Quantification Based on Radius of Curvature

Consider the parameter called a radius of curvature [73], as defined in Appendix B. A point in a point cloud has a radius of curvature, ρ_i, $i = 0, 1, \ldots$. To calculate ρ_i, the point itself and two more preceding consecutive points are needed. The variability in ρ_i is calculated for circle, ellipse, and spiral, as shown in Figures 11–13.

Figure 11 shows two point clouds of the same shape, circle. Figure 11a shows the point cloud of the circle modeled by Equation (A1), where the radius, $a = 100$ and center, $P_c = (150{,}150)$. In this case, 49 points are created to model the circle. Figure 11b shows the values of $\rho_{i,}$ which is equal to 100.21. Theoretically, ρ_i must be equal to $a = 100$. This small error ($100.21 - 100 = 0.21$) is due to calculation precision error. On the other hand, Figure 11c shows the point cloud of the same circle modeled by a PCA-generated point cloud. For this point cloud, $r_i = 100$ ($= d$); $\varphi = 0$; $\theta_i = 2\pi i/n$; $n = 48$; $i = 0, 1, \ldots$, 48; and $P_c = (150, 150)$. In this case as well, 49 points are created to model the circle. Figure 11d shows the values of ρ_i, which is equal to 100.21. This means that for a circle, r_i plays the role of the radius of curvature of a circle.

Figure 12 shows two point clouds of the same shape, ellipse. Figure 12a shows the point cloud of the ellipse modeled by Equation (A2), where the major radius, $a = 54$; minor radius, $b = 46$; and center, $P_c = (80, 80)$. In this case, 49 points are created to model the ellipse. Figure 12b shows the variation of ρ_i. On the other hand, Figure 12c shows the point cloud of the same ellipse modeled by a PCA-generated point cloud. For this point cloud, $d = 15$; $\varphi = 0$; r_i is decreased linearly from 54 to 46 and increased linearly from 46 to 56 for two cycles; $\theta_i = 2\pi i/n$; $n = 48$; $i = 0, 1, \ldots$, 48; and $P_c = (80, 80)$. In this case as well, 49 points are created to model the ellipse. Figure 12d shows the variation of ρ_i. As seen in Figure 12a,c, it is clear that both point clouds are identical and their radius of curvature (Figure 12b,d) also varies in the same trend. This means that for an ellipse, r_i plays the role of the radius of curvature of an ellipse.

Figure 13 shows two point clouds of the same shape, spiral. Figure 13a shows the point cloud of the spiral modeled by Equation (A3), where an arbitrary, positive, real constant, $a = 28.647$ that controls the distance between the successive turnings of the spiral. In this case, 49 points are created to model the spiral. Figure 13b shows the variation of ρ_i. On the other hand, Figure 13c shows the point cloud of the same spiral modeled by a PCA-generated point cloud. For this point cloud, $d = 15$; $\varphi = 0$; $r_i = 0$, 11.25, … , 540; $\theta_i = 2\pi i/n$; $n = 48$; $i = 0{,}1, \ldots$, 48; and $P_c = (600, 600)$. In this case as well, 49 points are created to model the spiral. Figure 13d shows the variation of ρ_i. As seen in Figure 13a,c, it is clear that both point clouds are identical and their radius of curvature (Figure 13b,d) also varies in the same trend. This means that for spiral, r_i plays the role of a radius of curvature of a spiral.

It is clear from Figures 11–13, the shape modeled by the parametric equation based and the PCA are visually identical. This means that the instantaneous distance plays the role of the radius of curvature when the shape is modeled by the PCA. The variation of the instantaneous distance is comparatively lower than the radius of curvature, which shows that the geometry of the shape can be easily controlled using the instantaneous distance compared to the radius of curvature. It is worth mentioning that there are several key elements for shape designing, and mathematical formulation of the radius of curvature or instantaneous distance can be one effective approach [74].

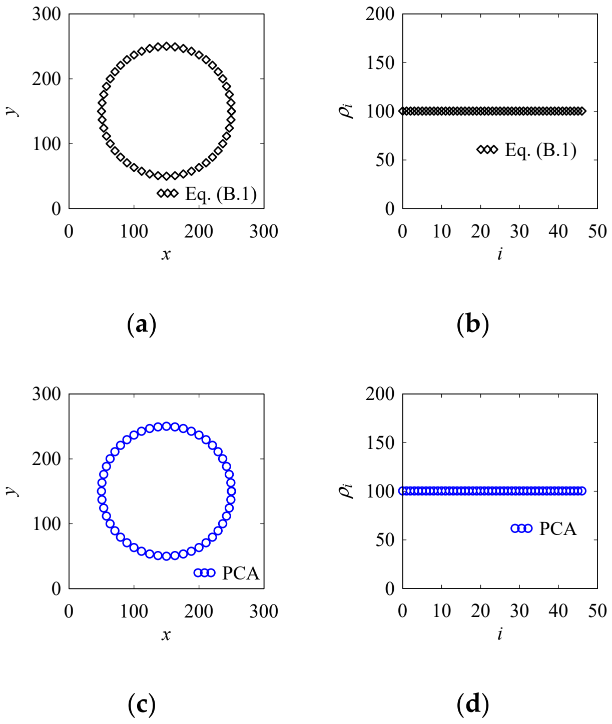

(**a**) (**b**)

(**c**) (**d**)

Figure 11. Circle shapes and their radii of curvature. (**a**) Point cloud of a circle modeled by a parametric equation; (**b**) radius of curvature of (**a**); (**c**) point cloud a circle modeled by the PCA; (**d**) radius of curvature of (**c**).

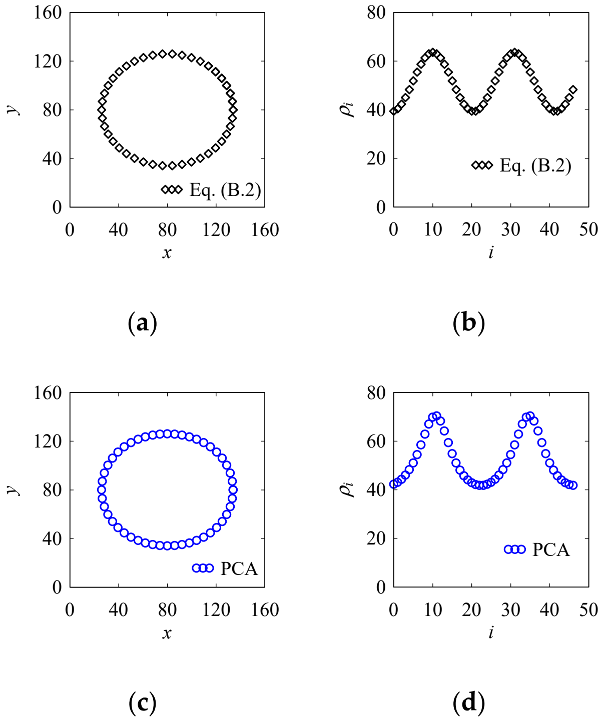

(**a**) (**b**)

(**c**) (**d**)

Figure 12. Ellipse shapes and their radii of curvature. (**a**) Point cloud of an ellipse modeled by a parametric equation; (**b**) radius of curvature of (**a**); (**c**) point cloud of an ellipse modeled by the PCA; (**d**) radius of curvature of (**c**).

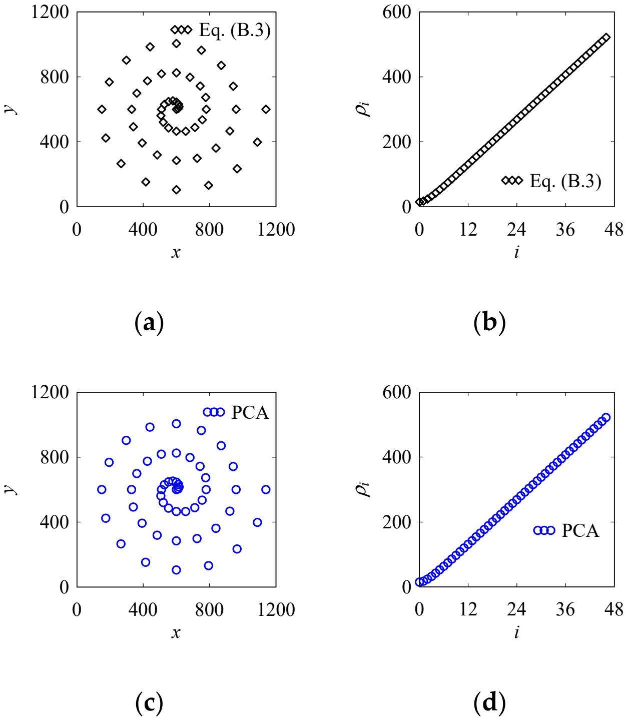

(**a**) (**b**) (**c**) (**d**)

Figure 13. Spiral shapes and their radii of curvature. (**a**) Point cloud of a spiral modeled by a parametric equation; (**b**) radius of curvature of (**a**); (**c**) point cloud of a spiral modeled by the PCA; (**d**) radius of curvature of (**c**).

3.2. Quantification Based on Aesthetic Value

This subsection describes the quantification of shapes based on a parameter called aesthetic value, denoted as α [75–77]. This parameter is defined in Appendix B. In order to know the aesthetic value, a plot called a logarithm curvature histogram (LCH) is used. The procedure to construct LCH for a given curve (in this case from a given point cloud) is also shown in Appendix B. For quantification of the aesthetic value, the ellipse and spiral shape are considered.

Figure 14a shows the point cloud of the ellipse modeled by Equation (A2), which is repeated from the previous section (Figure 12a). The corresponding LCH of the ellipse is shown in Figure 14b. Figure 14c shows the point cloud of the ellipse modeled by the PCA (repeated from Figure 12c). The corresponding LCH of the ellipse is shown in Figure 14d. Both point clouds have the same aesthetic value, α = 1.25. On the other hand, Figure 15a shows the point cloud of a spiral modeled by Equation (A3) (repeated from Figure 13a). The corresponding LCH of the spiral is shown in Figure 15b. Figure 15c shows the point cloud of the spiral modeled by the PCA (repeated from Figure 13c). The corresponding LCH of the spiral is shown in Figure 14d. Both point clouds of the spiral shape have the same aesthetic value, α = 1.22. As seen in Figures 14 and 15, even though the shapes are created using the PCA instead of the respective parametric equations, their aesthetic natures remain unaffected. It is also observed that the length of the line segment in the LCH depends on the variation range (minimum value to maximum value) of the radius of curvature. If the variation in the radius of curvature is high, the length of LCH becomes larger and vice versa.

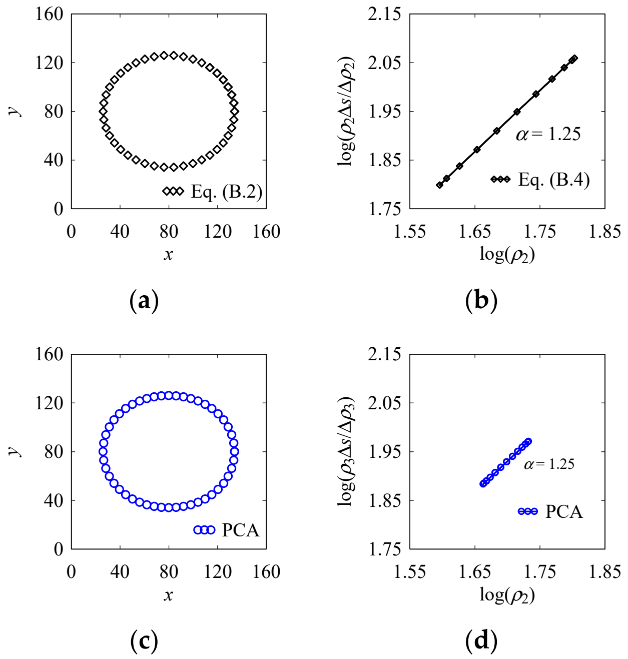

(**a**) (**b**)

(**c**) (**d**)

Figure 14. Logarithm curvature histogram (LCH) of ellipses. (**a**) Point cloud of an ellipse modeled by a parametric-based equation; (**b**) LCH of (a); (**c**) point cloud of an ellipse modeled by the PCA; (**d**) LCH of (c).

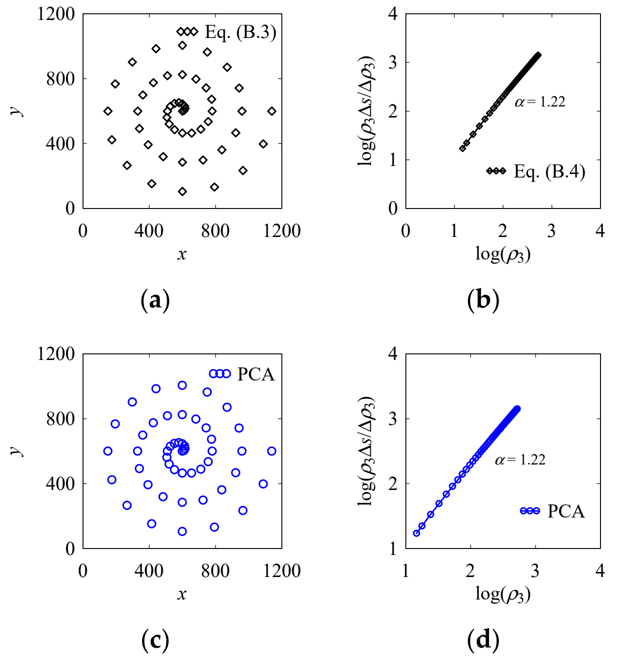

(**a**) (**b**)

(**c**) (**d**)

Figure 15. Logarithm curvature histogram of spirals. (**a**) Point of a spiral modeled by a parametric-based equation; (**b**) LCH of (**a**); (**c**) point cloud of a spiral modeled by the PCA; (**d**) LCH of (**c**).

4. 3D Solid Modeling and Physical Prototyping

Recall the last question, as follows. Does the deterministically created point cloud help create 3D solid models of some given objects?

In order to answer this question, this section presents an illustrative example where a relatively complex object is first modeled by some point clouds. The point clouds are generated by the PCA. The point clouds are used in a sequential order to produce a solid model of the object within a CAD package. Finally, a physical prototype is built from digital data of the solid model.

Figure 16a shows an ewer from Seto ware (Seto is a city located in Aichi Prefecture, Japan) produced during the Nanboku-chō period in the 13th century [78]. The ewer consists of three parts—the body, spout, and handle—as shown in Figure 16b. Few line segments and a concave can represent the body, line segments can represent the spout, and an elliptical shape can represent the handle. Hence, the ewer can be constructed using line segments, a concave curve, and an ellipse. Figure 16c shows the individual point clouds modeled by the PCA. Consider the individual point clouds, PC_1, PC_3, PC_4, PC_5, PC_6, PC_7, and PC_8, presenting the line segments that can be modeled by customizing the inputs, θ_i and r_i, as described in Section 2 (Figures 2 and 3). Similarly, consider the point cloud PC_9, presenting an elliptical shape that can be modeled by customizing the inputs, θ_i and r_i, as described in Section 2 (Figure 7). Regarding the point cloud PC_2, presenting the concave curve that can be modeled by setting the input parameters of the PCA as follows: PC = (90,90); d = 15; φ = 0; $\theta_i = \pi i/2n$, n = 30; i = 0,1, . . . , 30; and r_i is linearly decreased from 73.55 to 0.

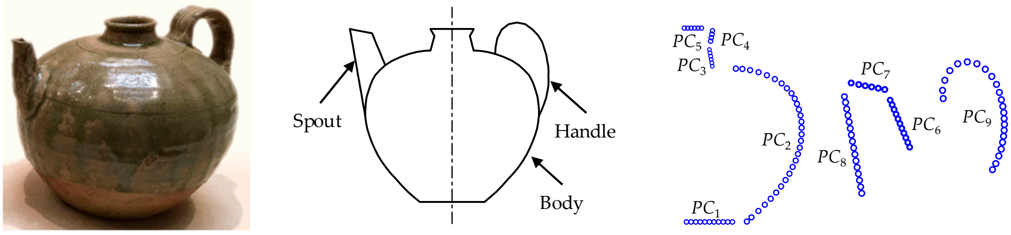

(**a**) (**b**) (**c**)

Figure 16. An Ewer from Seto ware. (**a**) A photograph of the Ewer [78]; (**b**) an illustration of the ewer; (**c**) individual point clouds.

The steps for solid CAD modeling are described as follows. In the first step, the individual point clouds PC_1, PC_2, PC_3, PC_4, and PC_5 are sequentially synthesized by a C^0 continuity approach which represents the basic point cloud of the ewer body. The resulting point cloud is shown in Figure 17a. These point clouds are then transferred to a commercially available 3D CAD package for solid modeling. By revolving the point cloud 360°, a solid CAD model of the ewer body is constructed. The result is shown in Figure 17b.

In the second step, the point clouds PC_6, PC_7, and PC_8 are sequentially synthesized by a C^0 continuity approach which represents the basic point cloud of the spout. The resulting point cloud is shown in Figure 18a. The point clouds are then injected into the solid CAD model of the body as shown in Figure 18b. Here, P_1 and P_2 represent the start point and endpoint of PC_7 and are connected to the endpoint of PC_6 and start point of PC_8, respectively. For the other points, P_3 denotes the endpoint of PC_8 and P_4 denotes the starting point of PC_6. The point clouds must be iterated so that P_3 and P_4 must lie on a tangent to the surface of the body. Taking P_1 and P_2 as reference points, plane 1 is created and then an ellipse is constructed on plane 1, as shown in Figure 18c. Similarly, taking P_3 and P_4 as reference points, plane 2 is created and then another ellipse is constructed on plane 2, as shown in Figure 18c. Now, these two ellipses are joined by applying the lofted function to form the spout, as shown in Figure 18d. Afterward, a hollow is created inside the solid CAD model by offsetting surface and hiding the solid body and applying the thicken function on the offset surface. The resulting solid CAD model is shown in Figure 18e.

In the third step, the point cloud PC_9, shown in Figure 19a, is injected on the solid CAD model, as shown in Figure 19b. In this case, PC_9 must iterate so the start point P_5, and endpoint P_6, must lie on the mid-section of the outer and inner surface of the body, shown in Figure 19b. Taking P_5 and PC_9 as a reference, plane 3 is created and then the ellipse is constructed on plane 3, as shown in Figure 19c. Then, applying the sweep function on the ellipse and taking PC_9 as a sweep path, a handle is created. The resulting solid CAD model is shown in Figure 19d.

Finally, the rendered solid CAD model of the ewer is shown in Figure 20a. Once the solid CAD modeling is done, triangulation modeling is performed simply by saving the solid CAD model into an STL data file using a CAD package. Figure 20b shows the triangulation model of the ewer. The STL data generated from the triangulation modeling can be used to build a physical model using commercially available 3D printing devices (e.g., 3D printer). Figure 20b shows one of the ewer physical models built by a 3D printer available at the Kitami Institute of Technology.

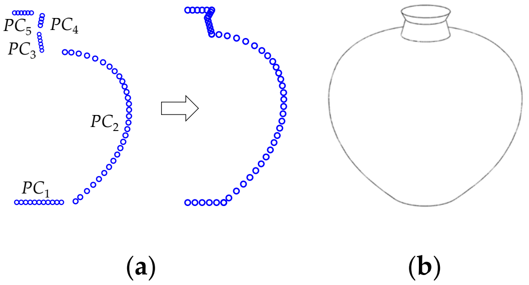

Figure 17. Solid CAD modeling of the ewer body. (**a**) Basic point cloud of the body; (**b**) solid CAD model constructed using the basic point cloud.

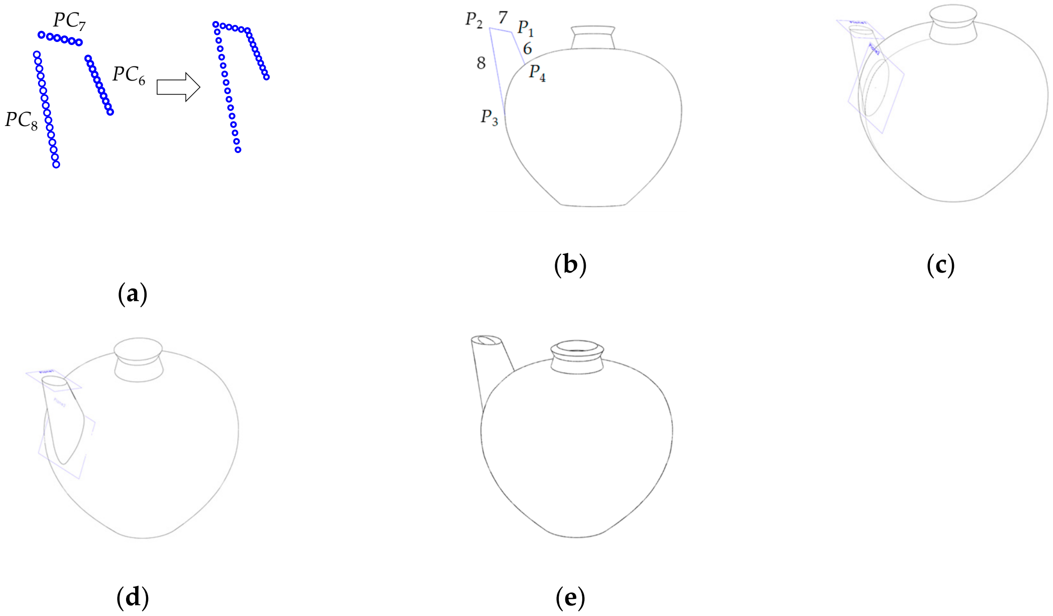

Figure 18. Solid CAD modeling of the ewer spout. (**a**) Basic point cloud of the spout; (**b**) point cloud of the spout injected into the solid CAD model; (**c**) reference planes and ellipses to construct spout; (**d**) result of spout construction; (**e**) a solid CAD model with hollow inside.

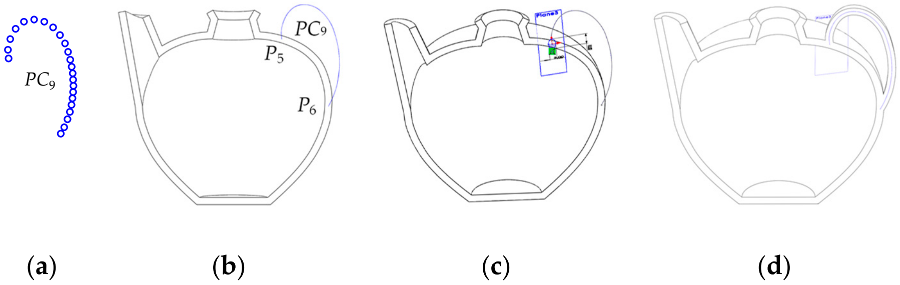

Figure 19. Solid CAD modeling of the ewer handle. (**a**) Point cloud of the handle; (**b**) point cloud of handle injected into the solid CAD model; (**c**) reference plane and ellipse to construct handle; (**d**) result of handle construction.

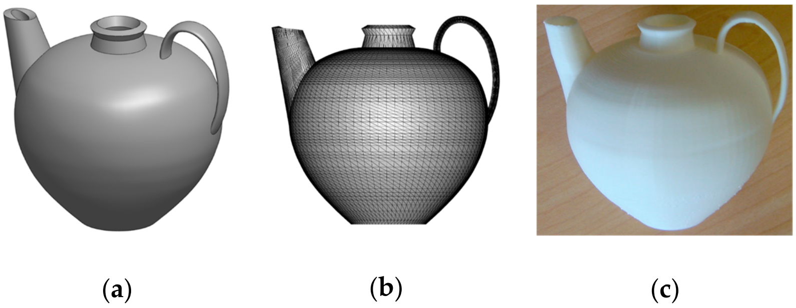

Figure 20. Ewer model. (**a**) Rendered solid CAD model; (**b**) triangulation model; (**c**) 3D printed model.

5. Discussions

The above three sections answer the questions coined in the introduction. Apart from this, the presented methodology can be used in many different ways. One of the ways is surface texturing. This section provides some insights into this type of surface texturing.

The PCA-based point cloud can be used for surface texturing. For example, consider the solid model of the ewer shown in Figure 20. A texture can be added to it. In this case, the PCA-based point cloud can be used. For example, consider the point clouds that represent a pattern taken from Ainu cultural heritage. The settings for creating the point clouds are available in [69].

Figure 21a shows the point cloud of the texture. This point cloud is injected into the solid CAD model of the ewer, as shown in Figure 21b. Then, the texture on the front side is constructed by extruding the point cloud from the surface of the ewer. The texture on the backside is constructed by mirroring the front side texture. The result is shown in Figure 21c. Finally, the physical model is realized using a 3D printer, as shown in Figure 21d.

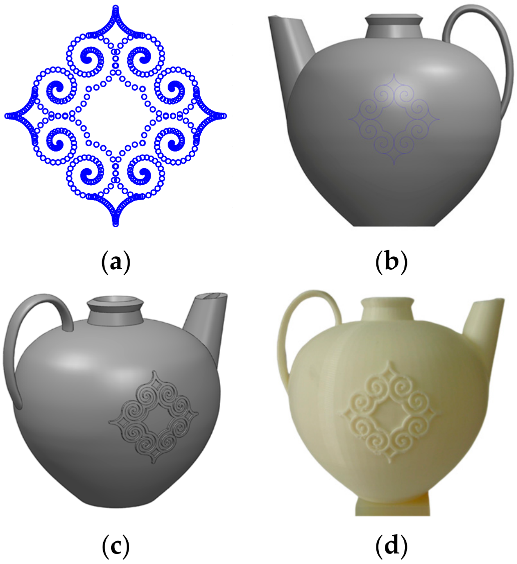

Figure 21. Surface texturing. (**a**) Point cloud of surface texture [69]; (**b**) point cloud of surface texture injected into the solid CAD model of ewer; (**c**) solid CAD model of the ewer with surface texture; (**d**) 3D printed physical model of the ewer with surface texture.

In addition to texturing, the 3D printed physical model of ewer shown in Figure 21 is scanned using a 3D scanner available at the Kitami Institute of Technology. Three different orientations are implemented to scan the ewer, as shown in Figure 22. Point clouds are then preprocessed (removing noise points, removing redundant points, and combining all point clouds into a single coordinate) and a triangulation model is created directly from the point cloud. The triangulation model is shown in Figure 22. Afterwards, a solid CAD model is constructed from the triangulation model. As seen in Figure 23a, the texture is a blur and there is also surface distortion near the handle. To make the texture sharp, clear, and have a smooth surface, it requires the user efforts while performing solid CAD modeling. It is worth mentioning that the triangulation model from the 3D scanned point cloud (Figure 23) consists of 271,803 facets and 815,409 vertices, whereas the triangulation model from the PCA-based point cloud has 25,336 facets and 76,008 vertices for the model without texture (Figure 20b); and 51,244 facets and 153,732 vertices for the model with texture (Figure 21d). It is clear that the 3D scanned point cloud has 10 times higher facets than the PCA-based point cloud. As a result, the 3D scan-based approach becomes user-dependent and requires heavy computation. Table 2 shows a summary of the number of points, facets, vertices, and printing time required to manufacture the physical model of the given ewer.

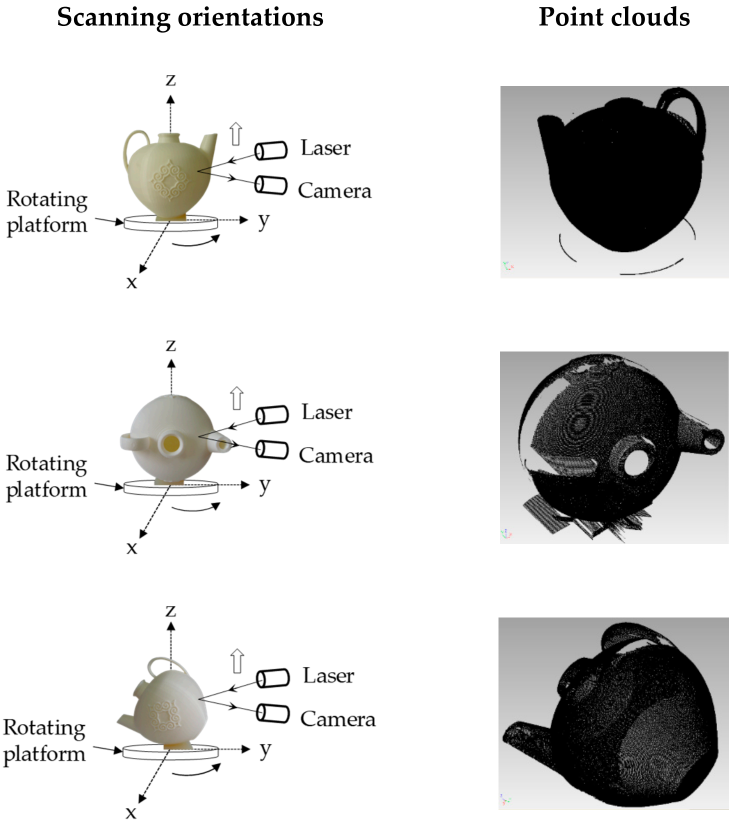

Figure 22. Point cloud registration from different orientations.

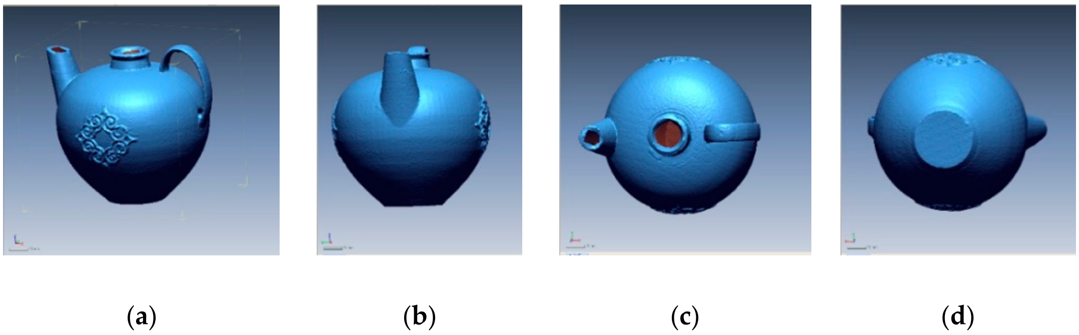

Figure 23. Triangulation model obtained from the 3D scan point cloud data set. (**a**) Front view; (**b**) side view; (**c**) top view; (**d**) bottom view.

The article has demonstrated geometric modeling of a given shape which is completely controlled by a few analytically generated points and free from computational complexity. This way, the user has the freedom to design any given shape without being dependent on the data acquisition system. Moreover, the point clouds are used in a sequential order to produce the solid CAD model of the given object.

Table 2. Summary of results for different models.

Models	**Model without Texture**	**Model with Texture**	**3D Scanned Model**
Number of points	109	789	52,1404
Number of facets	25,336	51,244	271,803
Number of vertices	76,008	153,732	815,409
Printing time without support	7 h, 50 min, 38 s	8 h, 6 min, 58 s	-
Printing time with support	12 h, 20 min, 28 s	13 h, 14 min, 56 s	-

6. Concluding Remarks

In this article, the characteristics and roles of the two variables (instantaneous distance and instantaneous rotational angle) and three constants (center point, initial angle, and initial distance) used in the recursive process that deterministically creates a point cloud are studied. It is found that varying the pair of the instantaneous distance and instantaneous rotational angle in different combinations can create many different shapes. For examples, in this study, a straight-line, circle, ellipses, spiral, astroid, S-shape, and leaf-shape are created using five different combinations of instantaneous distance and instantaneous rotational angle. The first constant (center point) can perform the function of translation in both x- and y-axis directions. The second constant (initial angle) can perform the function of rotation of shape around the center point. However, the third constant does not affect the shape to be modeled; it is only necessary for placing the starting point.

A planner shape can be modeled by a recursive-process-created point cloud and by a parametric-equation-created point cloud. If both point clouds are the same in terms of some quantitative measures, then it can be said that the recursive-process-based shape modeling approach is as good as the parametric-equation-based shape modeling approach. This is verified using three well-known shapes, namely, circle, ellipse, and spiral. In the verification process, the parameters called the radius of curvature and aesthetic value are used. It is observed that both point clouds of a given shape (one generated by the recursive process and the other generated by the parametric equation) have the same radius of curvature and aesthetic value. It is also found that the instantaneous distance plays the role of a radius of curvature. This means that it is not difficult to predict the values of the instantaneous distance compared to those of the radius of curvature while modeling an arbitrary shape.

In addition, an illustrative example that shows the efficacy of the recursive process in virtual and physical prototyping of a relatively complex 3D object is presented. The results show that, compared to a 3D-scanner-created point cloud, the recursive-process-created point cloud helps avoid computational complexity in reverse engineering. It also makes reverse engineering more systematic of complex shape. Moreover, the recursive-process-created point cloud can be used to perform surface texturing.

In the future, this study can be extended to develop a system that automatically generates a shape based on the user-defined inputs (instantaneous distance and rotational angle, and alike). This way, human cognition-based reverse engineering can be achieved—which is one of the frontiers of digital manufacturing.

Author Contributions: Tashi, A.M.M.S.U., and A.K. conceived the idea. Tashi and A.M.M.S.U. worked on the methodology and manuscript preparation. Tashi and A.K. conducted the scanning experiment in Section 5. Tashi and AM.M.S.U. produced the point cloud and solid CAD models. A.M.M.S.U. administered the work.

Acknowledgments: The authors acknowledge Kitami Institute of Technology for providing materials and financial support during the course of this study.

Conflicts of Interest: The authors declare no conflicts of interest.

Appendix A Point Cloud Creation Algorithm

The PCA needs three constants, namely, the center point (P_c), initial distance (d), and the initial angle (φ), that remain the same during the iterations. In addition, the PCA needs two variables—namely, the instantaneous rotational angle (θ_i) and instantaneous distance (r_i), i = 0, 1, ..., n—that change in every iteration. The PCA consists of four steps. The first is input, the second is calculation, the third is iteration, and the last is output. In the input step, $P_c = (P_{cx}, P_{cy}) \in \Re^2$; $d > 0$; $\varphi \in \Re$; $r_i \in \Re \mid i = 0$, 1, ..., n); and $\theta_i \in \Re \mid i = 0, 1, ..., n$ are defined. In the calculation step, an initial point $P_0 = (P_{0x}, P_{0y})$ is calculated first at distance d from P_c on line P_cP_0, making angle φ in the counterclockwise direction with the x-axis. In the iteration step, P_0 is rotated counterclockwise from the x-axis using θ_i to create points $P_i = (P_{ix}, P_{iy})$, $i = 0, 1, \ldots, n$. Afterward, points $P_i = (P_{ix}, P_{iy})$ are placed at a distance r_i from P_c resulting in points $P_{ei} = (P_{ix}, P_{iy})$, i = 0, 1, ..., n. In the output step, the points $P_{ei} = (P_{ix}, P_{iy})$, i = 0, 1, ..., n, are collected for creating the desired point cloud denoted as $PC = \{P_{ei} \mid i = 0, 1, ..., n\}$.

Point Cloud Creation Algorithm (PCA):		
1	*Define*:	Center Point $P_c = (P_{cx}, P_{cy}) \in \Re^2$, Initial Length $d > 0$, Initial Angle $\varphi \in \Re$ Instantaneous Distance ($r_i \in \Re \mid i = 0, 1, ..., n$) Instantaneous Rotational Angle ($\theta_i \in \Re \mid i = 0, 1, ..., n$)
2	*Calculate*:	$P_0 = (P_{0x}, P_{0y})$ so that $P_{0x} = P_{cx} + d\cos\phi$ and $P_{0y} = P_{cy} + d\sin\phi$
3	*Iterate*:	For i = 0, 1, ..., n Rotate P_0 by an angle θ_i around P_c in the counterclockwise direction to create $P_i = (P_{ix}, P_{iy})$ so that $P_{ix} = P_{cx} + (P_{0x} - P_{cx})\cos\theta_i - \left(P_{0y} - P_{cy}\right)\sin\theta_i,$ $P_{iy} = P_{cy} + (P_{0x} - P_{cx})\sin\theta_i + \left(P_{0y} - P_{cy}\right)\cos\theta_i.$ Extend P_i to P_{ei} (a point on the line P_cP_i at a distance r_i from P_c) $P_{eix} = P_{cx} + (P_{ix} - P_{cx})(r_i/d),$ $P_{eiy} = P_{cy} + \left(P_{iy} - P_{cy}\right)(r_i/d).$ End For
4	*Output*:	$PC = (P_{ei} \mid i = 0, 1, ..., n)$

Appendix B Definition of Relevant Shapes and Parameters

B.1. Relevant Shapes

Let the point clouds of a circle, ellipse, and spiral be modeled by three parametric equations. Each shape is given by a point cloud consisting of the points $P_i = \{(P_{xi}, P_{yi}) \mid i = 0, 1, \ldots, n$. The mathematical formulations of the shapes are as follows.

Consider a circle with radius a, where $a > 0$. Let $P_c = (P_{cx}, P_{cy})$ be the center of the circle on the x–y plane. An arbitrary point on the circumference of the circle is denoted as $P_i = \{(P_{xi}, P_{yi}) \mid i = 0, 1, \ldots, n\}$ and is given by

$$P_{xi} = P_{cx} + a\cos\theta_i, \quad P_{yi} = P_{cy} + a\sin\theta_i. \tag{A1}$$

In Equation (A1), $\theta_i = 2\pi i/n$. While creating a point cloud for a circle using Equation (A1), the parameters are set as follows: a = 100; n = 48; and i = 0, 1, ..., 48. The point cloud shown in Figure 11a presenting the circle is created using the abovementioned formulation.

Consider an ellipse with major radius a and minor radius b, where a, $b > 0$ and $a > b$. Let $P_c = (P_{cx}, P_{cy})$ be the center of the ellipse in the x–y plane. An arbitrary point on the circumference of the ellipse is denoted as $P_i = \{(P_{xi}, P_{yi}) \mid i = 0, 1, \ldots, n\}$ and is given by

$$P_{xi} = P_{cx} + a\cos\theta_i, \quad P_{yi} = P_{cy} + b\sin\theta_i. \tag{A2}$$

In Equation (A2), $\theta_i = 2\pi i/n$. While creating a point cloud for an ellipse using Equation (A2), the parameters are set as follows: $a = 54$; $b = 46$; $n = 48$; and $i = 0, 1, ..., 48$. The point cloud shown in Figure 12a presenting the ellipse is created using the abovementioned formulation.

Consider a spiral. Let it be an Archimedean spiral. Let $P_C = (P_{cx}, P_{cy})$ be the center of the spiral in the x–y plane. Consider a to be the arbitrary positive real constant that controls the distance between the successive turnings of the spiral. An arbitrary point on the circumference of the spiral is denoted as $P_i = \{(P_{xi}, P_{yi}) \mid i = 0, 1, \ldots, n\}$ and is given by

$$P_{xi} = P_{cx} + a\theta_i\cos\theta_i, \quad P_{yi} = P_{cy} + a\theta_i\sin\theta_i. \tag{A3}$$

In Equation (A3), $\theta_i = 6\pi i/n$. While creating a point cloud for a spiral using Equation (A3), the parameters are set as follows: a = 28.647; $n = 48$; and $i = 0, 1, ..., 48$. The point cloud shown in Figure 13a presenting the spiral is created using the abovementioned formulation.

B.2. Radius of Curvature

Let ρ_i be the instantaneous radius of curvature for point $P_i = \{(P_{xi}, P_{yi}) \mid i = 0, 1, \ldots, n\}$. Thus, the following relationship holds [73]:

$$\rho_i = \frac{\left(\left(\dot{x}_i\right)^2 + \left(\dot{y}_i\right)^2\right)^{3/2}}{\left|\left(\left(\dot{x}_i\right)\left(\ddot{y}_i\right) - \left(\dot{y}_i\right)\left(\ddot{x}_i\right)\right)\right|}. \tag{A4}$$

In Equation (A4), $\dot{x}_i = P_{xi+1} - P_{xi}$; $\dot{y}_i = P_{yi+1} - P_{xy}$; $\ddot{x}_i = \dot{x}_{i+1} - \dot{x}_i$; and $\ddot{y}_i = \dot{y}_{i+1} - \dot{y}_i$. The radii of curvature for the shapes described above are computed using Equation (A4).

B.3. Aesthetic Value

A parameter called aesthetic value, denoted as α, quantifies the aesthetic nature of a curve [75–77], which is driven from the radius of curvature (Equation A4) and the arc length of a given curve, as shown in Figure A1. As seen in Figure A1a, ρ, Δs, and $\Delta\rho$ are the radius of curvature, arc length, and change in the radius of curvature, respectively. The logarithmic plot of $\Delta s/(\Delta\rho/\rho)$ versus ρ, which is called Logarithmic Curvature Histogram (LCH), becomes a straight line, and its slope is used to calculate the value of α, as seen in Figure A1b. Therefore, the following relationship holds [76]:

$$\log\left(\frac{\Delta s}{\Delta\rho/\rho}\right) = \alpha\log(\rho) + c. \tag{A5}$$

In Equation (A5), c is a constant. By knowing the value of α, the degree of aesthetics of a given curve (shape) can be quantified.

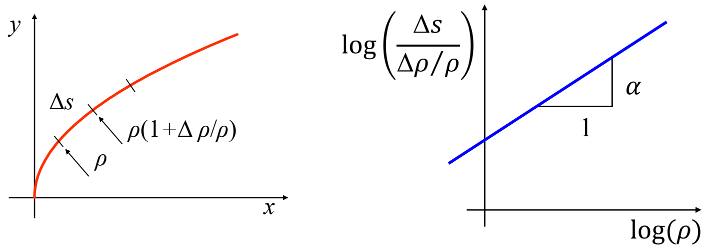

y
Δs
$\rho(1+\Delta\rho/\rho)$
ρ
x
$\log\left(\frac{\Delta s}{\Delta\rho/\rho}\right)$
α
1
$\log(\rho)$

(**a**) (**b**)

Figure A1. Determining aesthetic value. (**a**) Parameters for determining the aesthetic value; (**b**) calculating aesthetic value using LCH.

References

1. Thompson, M.K.; Moroni, G.; Vaneker, T.; Fadel, G.; Campbell, R.I.; Gibson, I.; Bernard, A.; Schulz, J.; Graf, P.; Ahuja, B.; et al. Design for Additive Manufacturing: Trends, opportunities, considerations, and constraints. *CIRP Ann.* **2016**, *65*, 737–760. [CrossRef]
2. Gibson, I.; Rosen, D.; Stucker, B. *Additive Manufacturing Technologies: 3D Printing, Rapid Prototyping, and Direct Digital Manufacturing*, 2nd ed.; Springer-Verlag: New York, NY, USA, 2015.
3. Gao, W.; Zhang, Y.; Ramanujan, D.; Ramani, K.; Chen, Y.; Williams, C.B.; Wang, C.C.L.; Shin, Y.C.; Zhang, S.; Zavattieri, P.D. The status, challenges, and future of additive manufacturing in engineering. *Comput. Aided Des.* **2015**, *69*, 65–89. [CrossRef]
4. Tofail, S.A.M.; Koumoulos, E.P.; Bandyopadhyay, A.; Bose, S.; O'Donoghue, L.; Charitidis, C. Additive manufacturing: scientific and technological challenges, market uptake and opportunities. *Mater. Today* **2018**, *21*, 22–37. [CrossRef]
5. Nooran, R. *3D Printing: Technology, Applications, and Selection*, 1st ed.; CRC Press: Boca Raton, FL, USA, 2018.
6. Camille, B. What are you printing? Ambivalent emancipation by 3D printing. *Rapid Prototyp. J.* **2015**, *21*, 572–581.
7. Bourell, D.L.; Rosen, D.W.; Leu, M.C. The Roadmap for Additive Manufacturing and Its Impact. *3D Print. Addit. Manuf.* **2014**, *1*, 6–9. [CrossRef]
8. Hirz, M.; Rossbacher, P.; Gulanová, J. Future trends in CAD—From the perspective of automotive industry. *Comput. Aided Des. Appl.* **2017**, *14*, 734–741. [CrossRef]
9. Yap, Y.L.; Tan, Y.S.E.; Tan, H.K.J.; Peh, Z.K.; Low, X.Y.; Yeong, W.Y.; Tan, C.S.H.; Laude, A. 3D printed bio-models for medical applications. *Rapid Prototyp. J.* **2017**, *23*, 227–235. [CrossRef]
10. Hieu, L.C.; Zlatov, N.; Vander Sloten, J.; Bohez, E.; Khanh, L.; Binh, P.H.; Oris, P.; Toshev, Y. Medical rapid prototyping applications and methods. *Assembly Autom.* **2005**, *25*, 284–292. [CrossRef]
11. Sun, W.; Starly, B.; Nam, J.; Darling, A. Bio-CAD modeling and its applications in computer-aided tissue engineering. *Comput. Aided Des.* **2005**, *37*, 1097–1114. [CrossRef]
12. Mannoor, M.S.; Jiang, Z.; James, T.; Kong, Y.L.; Malatesta, K.A.; Soboyejo, W.O.; Verma, N.; Gracias, D.H.; McAlpine, M.C. 3D Printed Bionic Ears. *Nano Lett.* **2013**, *13*, 2634–2639. [CrossRef]
13. Steffan, D.; Dominic, E. A CAD and AM process for maxillofacial prostheses bar-clip retention. *Rapid Prototyp. J.* **2016**, *22*, 170–177.
14. Luximon, Y.; Ball, R.M.; Chow, E.H.C. A design and evaluation tool using 3D head templates. *Comput. Aided Des. Appl.* **2016**, *13*, 153–161. [CrossRef]
15. Jung, W.; Park, S.; Shin, H. Combining volumetric dental CT and optical scan data for teeth modeling. *Comput. Aided Des.* **2015**, *67*, 24–37. [CrossRef]
16. Urbanic, R.J. From thought to thing: using the fused deposition modeling and 3D printing processes for undergraduate design projects. *Comput. Aided Des. Appl.* **2016**, *13*, 768–785. [CrossRef]
17. Galina, L.; Na, X. Academic library innovation through 3D printing services. *Libr. Manag.* **2017**, *38*, 208–218.
18. Heather, M.M.L. Makers in the library: case studies of 3D printers and maker spaces in library settings. *Libr. Hi Tech* **2014**, *32*, 583–593.
19. Wannarumon, S.; Bohez, E.L.J. A New Aesthetic Evolutionary Approach for Jewelry Design. *Comput. Aided Des. Appl.* **2006**, *3*, 385–394. [CrossRef]

20. 3D Printed Clothing. Available online: https://3dprint.com/tag/3d-printed-clothing/ (accessed on 13 September 2019).
21. The Future of Running is Here. Available online: https://www.newbalance.com/article?id=4041 (accessed on 13 September 2019).
22. 3D Printed Fashion: 10 Amazing 3D Printed Dresses. Available online: https://i.materialise.com/blog/3d-printed-fashion-dresses/ (accessed on 13 September 2019).
23. Nike. Nike Debuts First-ever Football Cleat Built Using 3D Printing Technology. Available online: https://news.nike.com/news/nike-debuts-first-ever-football-cleat-built-using-3d-printing-technology (accessed on 13 September 2019).
24. Sun, J.; Zhou, W.; Yan, L.; Huang, D.; Lin, L.Y. Extrusion-based food printing for digitalized food design and nutrition control. *J. Food Eng.* **2018**, *220*, 1–11. [CrossRef]
25. Lin, C. 3D Food Printing: A Taste of the Future. *J. Food Sci. Educ.* **2015**, *14*, 86–87. [CrossRef]
26. Ferreira, I.A.; Alves, J.L. Low-cost 3D food printing. *Ciência Tecnologia dos Materiais* **2017**, *29*, e265–e269. [CrossRef]
27. Jiang, H.; Zheng, L.; Zou, Y.; Tong, Z.; Han, S.; Wang, S. 3D food printing: Main components selection by considering rheological properties. *Crit. Rev. Food Sci. Nutr.* **2019**, *59*, 2335–2347. [CrossRef] [PubMed]
28. Lupton, D.; Turner, B. Food of the Future? Consumer Responses to the Idea of 3D-Printed Meat and Insect-Based Foods. *Food Foodways* **2018**, *26*, 269–289. [CrossRef]
29. Sakin, M.; Kiroglu, Y.C. 3D Printing of Buildings: Construction of the Sustainable Houses of the Future by BIM. *Energy Procedia* **2017**, *134*, 702–711. [CrossRef]
30. Hager, I.; Golonka, A.; Putanowicz, R. 3D Printing of Buildings and Building Components as the Future of Sustainable Construction? *Procedia Eng.* **2016**, *151*, 292–299. [CrossRef]
31. Lim, S.; Buswell, R.A.; Le, T.T.; Austin, S.A.; Gibb, A.G.F.; Thorpe, T. Developments in construction-scale additive manufacturing processes. *Autom. Constr.* **2012**, *21*, 262–268. [CrossRef]
32. Tay, Y.W.D.; Panda, B.; Paul, S.C.; Noor Mohamed, N.A.; Tan, M.J.; Leong, K.F. 3D printing trends in building and construction industry: A review. *Virtual Phys. Prototyp.* **2017**, *12*, 261–276. [CrossRef]
33. Scopigno, R.; Cignoni, P.; Pietroni, N.; Callieri, M.; Dellepiane, M. Digital Fabrication Techniques for Cultural Heritage: A Survey. *Comput. Graph. Forum* **2017**, *36*, 6–21. [CrossRef]
34. Sharif Ullah, A.M.M.; Sato, Y.; Kubo, A.; Tamaki, J.i. Design for Manufacturing of IFS Fractals from the Perspective of Barnsley's Fern-leaf. *Comput. Aided Des. Appl.* **2015**, *12*, 241–255. [CrossRef]
35. Várady, T.; Martin, R.R.; Cox, J. Reverse engineering of geometric models—An introduction. *Comput. Aided Des.* **1997**, *29*, 255–268. [CrossRef]
36. James, D.W.; Belblidia, F.; Eckermann, J.E.; Sienz, J. An innovative photogrammetry color segmentation based technique as an alternative approach to 3D scanning for reverse engineering design. *Comput. Aided Des. Appl.* **2017**, *14*, 1–16. [CrossRef]
37. Paulic, M.; Irgolic, T.; Balic, J.; Cus, F.; Cupar, A.; Brajlih, T.; Drstvensek, I. Reverse Engineering of Parts with Optical Scanning and Additive Manufacturing. *Procedia Eng.* **2014**, *69*, 795–803. [CrossRef]
38. Ullah, A.M.M.; Watanabe, M.; Kubo, A. Analytical Point-Cloud Based Geometric Modeling for Additive Manufacturing and Its Application to Cultural Heritage Preservation. *Appl. Sci.* **2018**, *8*, 656.
39. Furferi, R.; Governi, L.; Volpe, Y.; Puggelli, L.; Vanni, N.; Carfagni, M. From 2D to 2.5D i.e. from painting to tactile model. *Graph. Models* **2014**, *76*, 706–723. [CrossRef]
40. Rojas-Sola, J.I.; Galán-Moral, B.; De la Morena-De la Fuente, E. Agustín de Betancourt's Double-Acting Steam Engine: Geometric Modeling and Virtual Reconstruction. *Symmetry* **2018**, *10*, 351. [CrossRef]
41. Chen, Z.; Chen, W.; Guo, J.; Cao, J.; Zhang, Y.J. Orientation field guided line abstraction for 3D printing. *Comput. Aided Geom. Des.* **2018**, *62*, 253–262. [CrossRef]
42. Schwartz, A.; Schneor, R.; Molcho, G.; Weiss Cohen, M. Surface detection and modeling of an arbitrary point cloud from 3D sketching. *Comput. Aided Des. Appl.* **2018**, *15*, 227–237. [CrossRef]
43. Company, P.; Contero, M.; Conesa, J.; Piquer, A. An optimisation-based reconstruction engine for 3D modelling by sketching. *Comput. Graph.* **2004**, *28*, 955–979. [CrossRef]
44. Naya, F.; Conesa, J.; Contero, M.; Company, P.; Jorge, J. Smart Sketch System for 3D Reconstruction Based Modeling. In Proceedings of the Third International Symposium on Smart Graphics, Heidelberg, Germany, 2–4 July 2003; pp. 58–68.

45. Yang, J.; Cao, Z.; Zhang, Q. A fast and robust local descriptor for 3D point cloud registration. *Inf. Sci.* **2016**, *346–347*, 163–179. [CrossRef]
46. Li, W.; Song, P. A modified ICP algorithm based on dynamic adjustment factor for registration of point cloud and CAD model. *Pattern Recognit. Lett.* **2015**, *65*, 88–94. [CrossRef]
47. Jung, S.; Song, S.; Chang, M.; Park, S. Range image registration based on 2D synthetic images. *Comput. Aided Des.* **2018**, *94*, 16–27. [CrossRef]
48. Chen, Z.; Zhang, T.; Cao, J.; Zhang, Y.J.; Wang, C. Point cloud resampling using centroidal Voronoi tessellation methods. *Comput. Aided Des.* **2018**, *102*, 12–21. [CrossRef]
49. Skrodzki, M.; Jansen, J.; Polthier, K. Directional density measure to intrinsically estimate and counteract non-uniformity in point clouds. *Comput. Aided Geom. Des.* **2018**, *64*, 73–89. [CrossRef]
50. Lee, K.H.; Woo, H. Direct integration of reverse engineering and rapid prototyping. *Comput. Ind. Eng.* **2000**, *38*, 21–38. [CrossRef]
51. Budak, I.; Vukelić, D.; Bračun, D.; Hodolič, J.; Soković, M. Pre-Processing of Point-Data from Contact and Optical 3D Digitization Sensors. *Sensors* **2012**, *12*, 1100–1126. [CrossRef]
52. Masuda, H.; Niwa, T.; Tanaka, I.; Matsuoka, R. Reconstruction of Polygonal Faces from Large-Scale Point-Clouds of Engineering Plants. *Comput. Aided Des. Appl.* **2015**, *12*, 555–563. [CrossRef]
53. Williams, R.M.; Ilieş, H.T. Practical shape analysis and segmentation methods for point cloud models. *Comput. Aided Geom. Des.* **2018**, *67*, 97–120. [CrossRef]
54. Fayolle, P.-A.; Pasko, A. An evolutionary approach to the extraction of object construction trees from 3D point clouds. *Comput. Aided Des.* **2016**, *74*, 1–17. [CrossRef]
55. Pan, M.; Tong, W.; Chen, F. Phase-field guided surface reconstruction based on implicit hierarchical B-splines. *Comput. Aided Geom. Des.* **2017**, *52–53*, 154–169. [CrossRef]
56. Feng, C.; Taguchi, Y. FasTFit: A fast T-spline fitting algorithm. *Comput. Aided Des.* **2017**, *92*, 11–21. [CrossRef]
57. Peternell, M.; Steiner, T. Reconstruction of piecewise planar objects from point clouds. *Comput. Aided Des.* **2004**, *36*, 333–342. [CrossRef]
58. Toll, B.; Cheng, F. Surface Reconstruction from Point Clouds. In Proceedings of the International Conference on Sculptured Surface Machining (SSM98), Chrysler Technology Center, MI, USA, 9–11 November 1998; Olling, G.J., Choi, B.K., Jerard, R.B., Eds.; Springer US: Boston, MA, USA, 1999; pp. 173–178.
59. Pralay, P. An easy rapid prototyping technique with point cloud data. *Rapid Prototyp. J.* **2001**, *7*, 82–90.
60. Ma, J.; Chen, J.S.-S.; Feng, H.-Y.; Wang, L. Automatic construction of watertight manifold triangle meshes from scanned point clouds using matched umbrella facets. *Comput. Aided Des. Appl.* **2017**, *14*, 742–750. [CrossRef]
61. Zhong, S.; Yang, Y.; Huang, Y. Data Slicing Processing Method for RE/RP System Based on Spatial Point Cloud Data. *Comput. Aided Des. Appl.* **2014**, *11*, 20–31. [CrossRef]
62. Chang, M.C.; Leymarie, F.F.; Kimia, B.B. Surface reconstruction from point clouds by transforming the medial scaffold. *Comput. Vis. Image Underst.* **2009**, *113*, 1130–1146. [CrossRef]
63. Remil, O.; Xie, Q.; Xie, X.; Xu, K.; Wang, J. Surface reconstruction with data-driven exemplar priors. *Comput. Aided Des.* **2017**, *88*, 31–41. [CrossRef]
64. Percoco, G.; Galantucci, L.M. Local-genetic slicing of point clouds for rapid prototyping. *Rapid Prototyp. J.* **2008**, *14*, 161–166. [CrossRef]
65. Wang, X.; Hu, J.; Guo, L.; Zhang, D.; Qin, H.; Hao, A. Feature-preserving, mesh-free empirical mode decomposition for point clouds and its applications. *Comput. Aided Geom. Des.* **2018**, *59*, 1–16. [CrossRef]
66. Yang, P.; Schmidt, T.; Qian, X. Direct Digital Design and Manufacturing from Massive Point-Cloud Data. *Comput. Aided Des. Appl.* **2009**, *6*, 685–699. [CrossRef]
67. Oropallo, W.; Piegl, L.A.; Rosen, P.; Rajab, K. Point cloud slicing for 3-D printing. *Comput. Aided Des. Appl.* **2018**, *15*, 90–97. [CrossRef]
68. Oropallo, W.; Piegl, L.A.; Rosen, P.; Rajab, K. Generating point clouds for slicing free-form objects for 3-D printing. *Comput. Aided Des. Appl.* **2017**, *14*, 242–249. [CrossRef]
69. Ullah, A.M.M. Symmetrical Patterns of Ainu Heritage and Their Virtual and Physical Prototyping. *Symmetry* **2019**, *11*, 985.
70. Ullah, A.M.M.S.; Omori, R.; Nagara, Y.; Kubo, A.; Tamaki, J. Toward Error-free Manufacturing of Fractals. *Procedia CIRP* **2013**, *12*, 43–48. [CrossRef]

71. Ullah, A.M.M.S.; D'Addona, D.M.; Harib, K.H.; Kin, T. Fractals and Additive Manufacturing. *Int. J. Autom. Technol.* **2016**, *10*, 222–230. [CrossRef]
72. Sharif Ullah, A.M.M. Design for additive manufacturing of porous structures using stochastic point-cloud: a pragmatic approach. *Comput. Aided Des. Appl.* **2018**, *15*, 138–146. [CrossRef]
73. Kishan, H. *Diffrential Calculus*; Atlantic Publishers & Distributors Pvt. Ltd.: New Delhi, India, 2007.
74. Ujiie, Y.; Matsuoka, Y. Macro-informatics of cognition and its application for design. *Adv. Eng. Inform.* **2009**, *23*, 184–190. [CrossRef]
75. Harada, T. Study of Quantitative Analysis of the Characteristics of a Curve. *Forma* **1997**, *12*, 55–63.
76. Miura, K.T.; Sone, J.; Yamashita, A.; Kaneko, T. Derivation of a General Formula of Aesthetic Curves. In Proceedings of the 8th International Conference on Humans and Computer (HC2005), Aizu-Wakamutsu, Japan, 31 August–2 September 2005; pp. 166–171.
77. Yoshida, N.; Saito, T. Interactive aesthetic curve segments. *Vis. Comput.* **2006**, *22*, 896–905. [CrossRef]
78. Japanese Pottery and Porcelain. Available online: https://en.wikipedia.org/w/index.php?title=Japanese_pottery_and_porcelain&oldid=875182192 (accessed on 13 September 2019).